3D Printing Concrete on temporary surfaces

The design and fabrication of a concrete shell structure

Borg Costanzi, C.; Ahmed, Z. Y.; Schipper, H. R.; Bos, F. P.; Knaack, U.; Wolfs, R. J.M.

DOI
10.1016/j.autcon.2018.06.013

Publication date
2018

Document Version
Accepted author manuscript

Published in
Automation in Construction

3D Printing Concrete on temporary surfaces: The design and fabrication of a concrete shell structure

C. Borg Costanzi, Z.Y. Ahmed, H.R. Schipper*, F.P. Bos**, U. Knaack, R.J.M. Wolfs

TU Delft, Faculty of Civil Engineering and Geosciences, Building 23, Stevinweg 1, 2628CN Delft, Netherlands
TU Eindhoven, Dept. Built Environment, Structural Design, 5612, AZ, Eindhoven, Netherlands

ARTICLE INFO

Keywords:
Concrete additive manufacturing
Shell structure
Adaptable mould

ABSTRACT

One of the geometrical restrictions associated with printed paste materials such as concrete, is that material must be self-supporting during printing. In this research paper a new methodology for 3D Printing Concrete onto a temporary freeform surface is presented. This is achieved by setting up a workflow for combining a Flexible Mould developed at TU Delft with a 4-degrees-of-freedom gantry printer (4 DOF) provided at TU Eindhoven. A number of hypothetical cases are studied, namely fully-printing geometries or combining 3D printing with casting concrete. The final outcome is a 5 m^2 partially-printed and partially-cast shell structure, combined with a CNC-milled mould simulating a Flexible Mould.

1. Introduction

Elements printed in concrete are generally achieved by extruding wet paste-material in layers which eventually build up the desired shape. While this allows for complex elements to be realized in a more efficient method compared to traditional fabrication techniques, there still are some major restrictions using concrete additive manufacturing. Because material is extruded in a wet-state, the build-up of layers must be such that they are self-supporting in order to avoid collapse, imposing somewhat of a restriction on possibilities for realizing geometry. The concept of providing a temporary surface for printing is a re-occurring theme in a multitude of Additive Materials. Tam et al. [1] have developed a method for robotically printing thermoplastics onto a wooden mould. Their study, Stress-Line-Additive-Manufacturing (SLAM), consists of converting stress-lines into splines which are used to define print paths onto a CNC-milled mould surface. Seyedahmadian et al. [2] adopted a similar study for developing an automated process for pressing fibrous materials onto a wooden mould. This method of pressing fibrous materials onto a temporary surface was further explored by Doerstelmann et al. [3] for the 2014 ITKE Research Pavilion at the University of Stuttgart. In this case, an inflated membrane was used to define an enclosed space. Lim et al. [12] used Curved Layered Fused Deposition Modelling (CLFDM) in combination with concrete additive manufacturing. This allowed for print paths to be generated to follow the curvature of a free-form surface, resulting in better surface quality, shorter printing time and higher surface strengths.

The aim of this research is to present a strategy for providing temporary support for extruded concrete. While there already has been some research related to the topic of temporary concrete support, this is usually achieved by using granular material such as sand [4]. This paper presents an alternative method that makes use of a silicone surface acting as a temporary support. The adaptable mould [5] used in this study is a flexible surface defined by adjusting an underlying pin-bed (Figs. 1–5).

The end result is a 2.5 m × 2.5 m shell structure consisting of complex interlocking geometries. A completely digital design to fabrication workflow was adopted by using a single software package for form-finding, optimization, generation of G-Code and communication with a Gantry Printer. This was achieved by using Rhinoceros 3D and Grasshopper (with plug-ins Karamba 3D and Galapagos).

The paper is organized in the following fashion: A brief description of the experimental setup is given in Section 2 and an overview of the production technique is outlined in Section 3. Sections 5 presents the general automated workflow adopted for the study. The form-finding strategy based on these is presented in Section 7. Sections 8 and 9 show the results of printing prototype and final shell structures whose assembly process is presented. Finally, the paper is concluded in Sections 9 and 10.

* Correspondence to: H.R. Schipper, Technische Universiteit Delft, Faculty of Civil Engineering and Geosciences, Department Materials, Mechanics, Management & Design (3Md), Building 23 - Room S2 1.55, Stevinweg 1, PO-box 5048, 2628 CN Delft, Netherlands.

** Correspondence to: F. Bos, Department of the Built Environment (Structural Design), Technische Universiteit Eindhoven, P.O. Box 513, 5600, MB, Eindhoven, Netherlands.

E-mail addresses: h.r.schipper@tudelft.nl (H.R. Schipper), F.P.Bos@tue.nl (F.P. Bos).

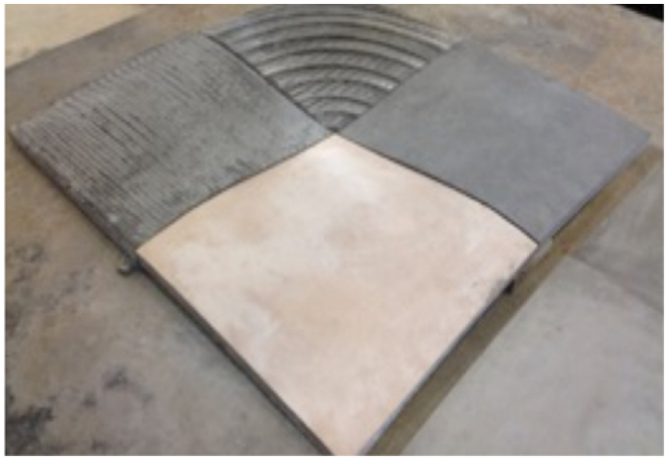

Fig. 1. 3D Concrete Printing that uses a CLFDM approach to generate layers. Source: Lim et al. [12].

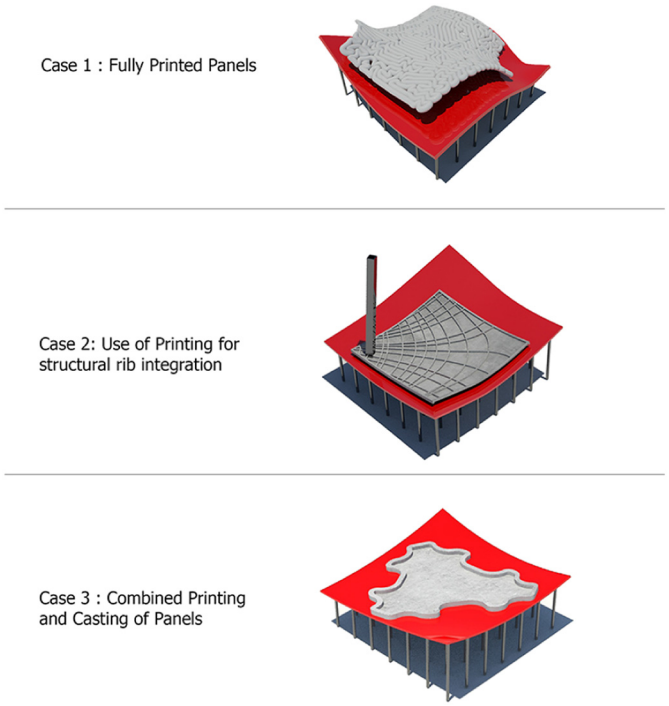

Fig. 2. Presentation of different cases for fully printed panels and partially-printed panels.

A number of potential areas of focus were outlined at the start of the study. These are classified in three distinct cases described as follows:

Case 1. Fully-Printed Panels. In this scenario it is imagined that architectural free-form cladding elements can be fully-printed onto a temporary surface. The figure below illustrates the potentials of using differential growth algorithms in combination with an adaptable mould to realize architectural panels. This concept was evidenced in previous studies including Lim et al. [12] and Borg Costanzi et al. [6].

Case 2. Combined printing for the integration of structural ribs. In this method, it is proposed that stresslines are converted into printing paths. A closed envelope is achieved by either first printing ribs and casting concrete in the voids or printing ribs onto an already-cast surface.

Case 3. combined printing and casting: complex geometry. The application adopts Additive Manufacturing to define a complex outer perimeter into which concrete is then cast.

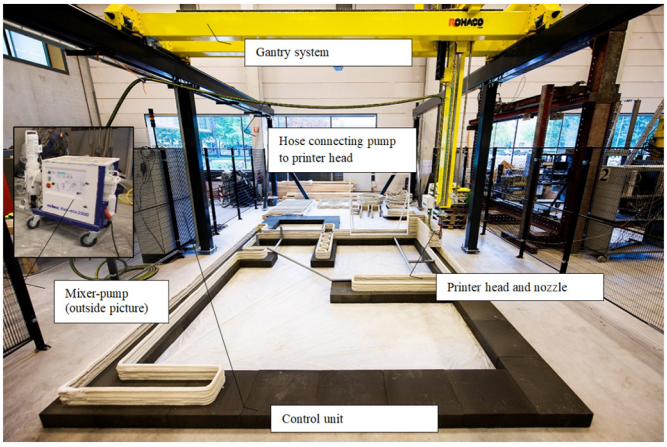

Fig. 3. 4 DOF Concrete Printer used at TU Eindhoven. Source: Bos et al. [7].

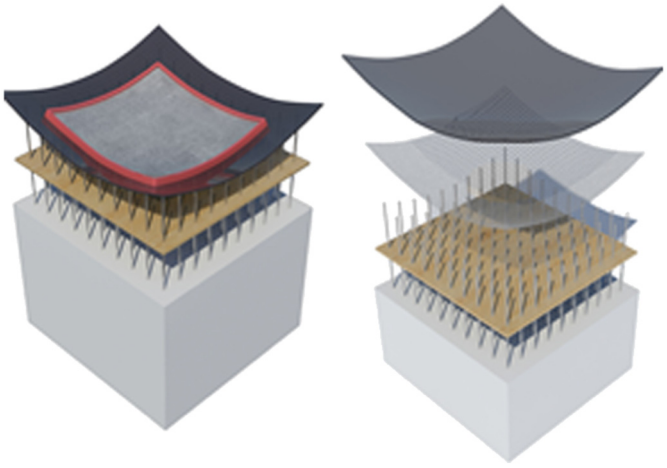

Fig. 4. Schematic of adaptable mould developed by Schipper [5].

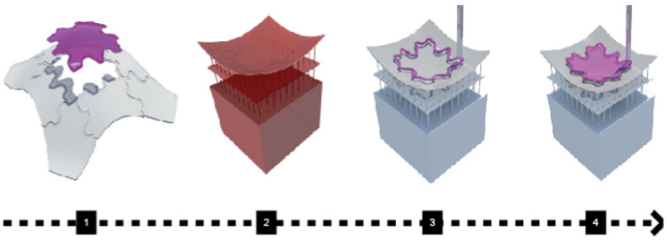

Fig. 5. Proposed production technique.

2. Experimental setup

The experimental setup consists of the following:

a. A 4-Degree of Freedom Gantry Printer (4 DOF). The use of an additional 4th axis to a 3-Axis printer allowed for the printing nozzle to be continuously oriented perpendicular with the printing path. The major advantage of orienting the nozzle towards the print path is that the extruded filament geometry could be controlled to a high degree.

b. An Adaptable Mould layout consists of a Deformable Steel mesh attached to a 1 m × 1 m pin bed [5]. Pins are spaced equidistantly at 220 mm distances and are adjusted in height to deform the steel mesh. A final silicone sheet is attached to the steel mesh to allow for a smooth finish of cast concrete.

3. Production technique

The production workflow consists of four key steps. These were kept digital to as great an extent as possible and can be summarized as follows:

a. 3D Geometry is converted into splines using Grasshopper and Rhinoceros. In the case studied for this research, it is the perimeter of the geometry that is converted into a spline.
b. The geometry is digitally oriented onto a simulation of the adaptable mould using a genetic algorithm to have the flattest orientation. The pin-heights are extracted from the digital model and used to adjust the physical mould.
c. The perimeter of the geometry is printed onto the calibrated adaptable mould in pre-determined layer heights.
d. Concrete is cast into the 3D printed perimeter and demolded after 24 h of curing.

This was an automated-process in theory; however a degree of manual labor was needed in practice. Although realizations of adaptable moulds already exist to allow for automated control of pin-heights, as shown by Vollers [13] and Adapa [8], the pins used in this setup were adjusted manually. This was largely due to equipment availability yet considered acceptable as it was not in the scope of the research to have an automated pin-bed as the focus was on printing onto a deformed surface.

4. Digital workflow

A completely digital workflow was envisaged for the research. This was maintained, except for the automation of pin-adjustment in the adaptable mould.

Step 1: geometry definition

The geometry used for printing was informed through a series of studies on the physical restrictions of the 3D Printer. The maximum angle concrete could be printed on as well as minimum turning radius of the printer were used as variables in the form-finding process of the final printing shape. The process of studying these variables is further discussed in Section 8.

Step 2: orientation of the adaptable mould

The geometry to be printed is digitally oriented onto the digital mould using Grasshopper. An evolutionary Algorithm engine, *Galapagos*, is used to find the most optimal positioning onto the adaptable mould.

This is repeated until the positioning is such that the mould undergoes the least amount of deformation. The minimal deformation of the mould is obtained by generating a bounding box for each rotation position and measuring the total deviation, Δh, between bounding box faces as shown in Fig. 6.

Galapagos, an evolutionary algorithm solver for Grasshopper, is used to simultaneously vary the rotations about the XY, XZ and YZ Axes (*Genomes*) while recording the values for deviation h1 (*fitness*). The axes angles for the smallest recorded value of h1 are stored and used for the final positioning of the mould. This gives the ideal orientation of the adaptable mould with the minimal inclination angle.

Step 3: adjusting of physical mould

The adjustment of the mould is the only non-fully-automated step in the process. Though it is possible to automate the adjustment of the mould pin beds, this would have implied excessive unnecessary costs to the project. In this scenario, it is imagined that servo motors are attached to every pin and adjusted through the parametric model using Firefly as a controller. For the actual setup used, pin heights are generated for the geometry positioned as described in step 5.3. These values are streamed and organized as a .txt file directly from the grasshopper file and the heights are then manually adjusted.

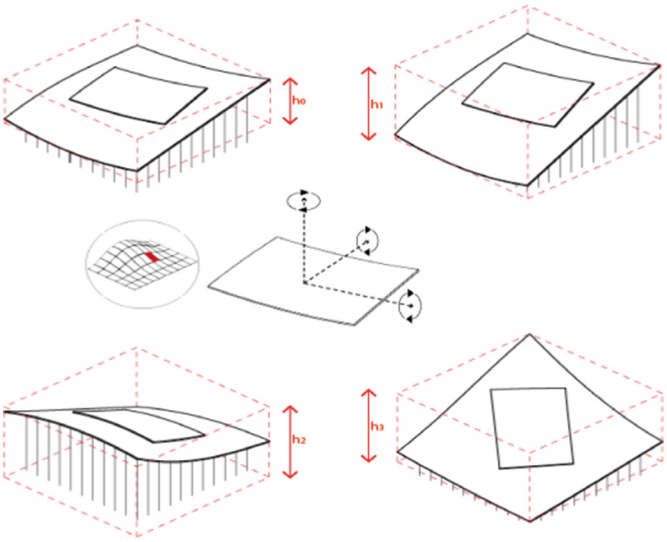

Fig. 6. Orientation of the mould to obtain minimum inclination.

Step 4: generating print path Gcode

Conventional 3D printers make use of slicing software to generate print paths. These generally slice a 3D geometry into a number of horizontal layers that are printed parallel to a XY base plane. This approach to generating print paths is not possible for this study due to the print-paths now being oriented along the face of a free-form surface and not a fixed XY plane. An alternative strategy was developed for generating G-code for printing onto a curved surface. The first print layer is defined as a spline which follows the contours of the free-form surface that defines its shape. This initial layer defines the geometry with a thickness equal to the layer heights. Additional layers are printed by shifting the initial spline by a distance equal to the layer printing thickness in the Z direction. This is repeated until the desired number of layers is achieved and is finalized by joining all the splines into a single print path. This approach was also utilized in other similar studies such as Lim et al. [12] and Borg Costanzi et al. [6] (Figs. 7–9).

Step 5: dividing the spline

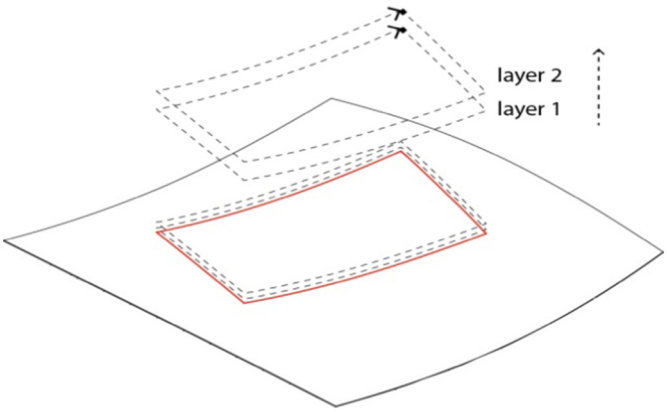

Fig. 7. Template for communication with printer.

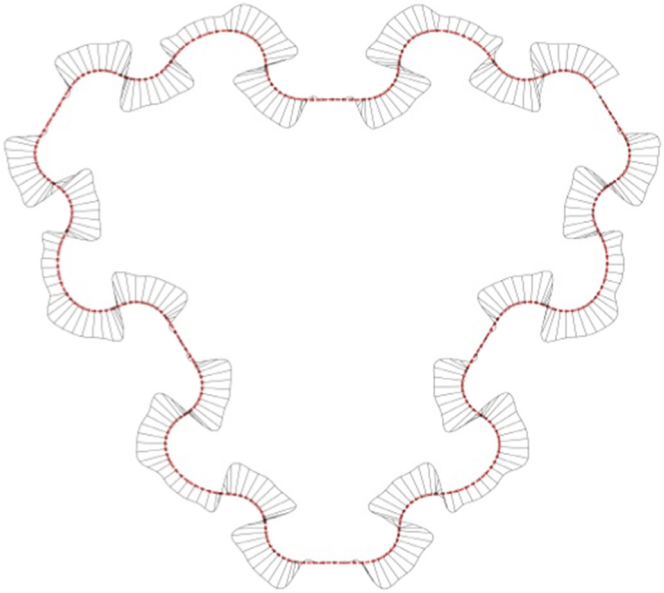

Fig. 8. Division of Print path according to curvature.

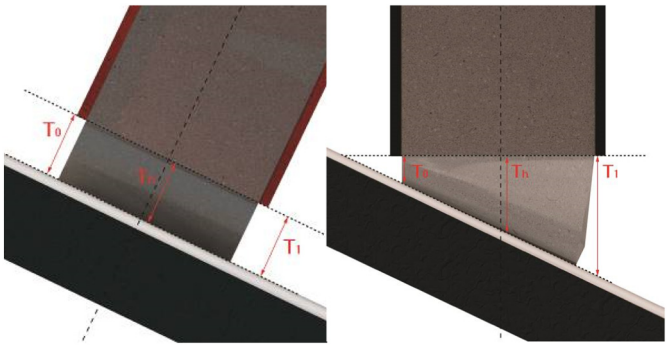

Fig. 9. [Left] showing constant nozzle offset printing perpendicular to surface. [Right] Variation in nozzle height when printing perpendicular to a horizontal axis.

In order to be converted into G-Code, the print path spline has to be divided into a number of points. These points are exported as Co-Ordinates which are communicated with the printer. In order to avoid unnecessary large files, a strategy for minimizing the number of division points was developed to divide the spline by its curvature. This is achieved by analyzing the rate of change in curvature on a given spline, initially interpolated by a defined number of points. The points are re-distributed along the spline depending on the curvature of a particular spline. The figure below shows the principle where an increase in curvature results in an increase in the number of division points.

Step 6: correction script

Using a 4 DOF (TX, TY, TZ, RZ) printer implies that the printer nozzle is kept perpendicular to a horizontal plane. The consequence of this when printing on a curved surface is that a constant nozzle distance cannot be maintained, as seen in Fig. 9. This is because the distance between the nozzle and the printing surface varies along the length of the nozzle. A correction script was developed to compensate for this limitation of the machinery used.

As shown in Fig. 9, collision between the printer and printing surface is likely to occur unless this variation in height is compensated for. This is done in two ways:

- Shifting the entire spline upwards by a pre-determined margin of safety. This approach was used initially as it was the most straightforward. However the result was that variation in printing heights (measured from the closest point) varied between 1 cm in the steepest areas and 6 cm in the shallowest areas. This had a drastic effect on the final print quality.
- Shifting the spline locally. This was the approach used in the final definition. Each spline division point was analyzed for any collisions with the surface. The point was then shifted in the Z direction by amount [Th + T0] as seen Fig. 10. A spline is then re-interpolated between the shifted points to produce a corrected print-path. The result was a far smoother and consistent print path with a deviation in nozzle height (measured from the closest point) between 2 cm and 2.5 cm.

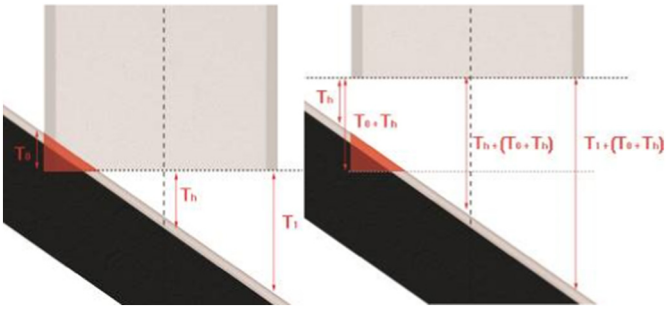

Fig. 10. Function used for providing a constant offset between the surface and nozzle achieved at a local level.

5. Shell prototype: parameter study

The results of this study are exhibited in the form of a 2.5 m × 2.5 m shell structure. To maintain a focused and restricted study, the final form is informed though the study of the following variables:

a. Minimum printing radius of the printer
b. Maximum inclination Angle onto which concrete can be printed.

5.1. Minimum printing radius

Printing right angles with an acceptable level of quality was not possible using the setup adopted. This is largely due to the printer temporarily slowing down when reaching a corner, resulting in stretching and overlap of extruded filaments in these areas. An acceptable level of quality was achieved where no overlap or stretching of extruded filament was evident. A series of tests were performed on both flat geometries as well as those printed onto an adaptable mould, highlighted in Fig. 11. Turning radii were varied until an acceptable level of quality was achieved.

As shown in Fig. 11 printing at too-small turning radii causes the printed filament to overlap on itself. This is because moving along a tight curve causes the printer to slow down while maintaining the same extrusion rate. The result is that more material is extruded than is needed and a ruined corner detail. An initial minimum turning radius was taken as 100 mm. However, as displayed in Fig. 11, this was still found to be too small an acceptable radius and was increased to 150 mm for the final structure.

5.2. Maximum inclination angle

The second variable studied was the maximum slope that the concrete could be printed on before sliding or tearing apart. Testing to understand the effects of printing at an inclination was carried out by printing a series of strips along differently-inclined surfaces. In his article on rheology, [9] describes the situations where concrete is cast on an inclination. It was stated that the critical internal shear strength of

Fig. 11. Initial printing tests. [Left] Flat Geometry with 80 mm radius [right] 100 mm radius on flexible mould [bottom] flat with varying radii.

the mixture to be stable may be expressed as:

$$\tau_{0;crit} = \rho \cdot g \cdot h \cdot \sin\varnothing$$

where:

h is the thickness of the concrete layer,
∅ is the angle of inclination of the slope,
ρ is the density of material.

For this setup, 3 layers having a height of 0.095 m were used, thus a total h of 0.0285 m. The inclination of the slope varied between 10° and 40°. The concrete mix had an estimated density of 2300 kg/m^3. Thus, the following range of values can be extrapolated for the two extreme angles of 10° and 40° respectively:

$$\tau_{0\,(10);crit} = 2300 \cdot 9.81 \cdot 0.0285 \cdot \sin 10^o = 111 \text{ Pa}$$

$$\tau_{0\,(40);crit} = 2300 \cdot 9.81 \cdot 0.0285 \cdot \sin 40^o = 413 \text{ Pa}$$

These values are shown to be in the lower boundaries that are required for a stable slope. Even should the real values be higher than what was calculated, the slope will also remain stable. If seen as lower boundaries, with a chance that the real values are even higher, the results are in line with the values that can be expected for a mixture with a rather stiff consistency. Both Wallevik [10] and Mueller [11] describe various tests in which the slump value and shear strength (in his article referred to as yield stress) are related. For zero- or low-slump concrete (as the concrete that is coming from the 3D-printer), values in the same order of magnitude (or higher) are found as the values calculated above. The Coulomb-friction between the mould and the concrete can be derived by dividing this friction by the vertical pressure, a Coulomb (dry-)friction coefficient μ is obtained with the value: $\mu = \tau_0/\sigma_v = \sin\theta = 0.174$ to 0.64. Probably the dry-friction model is not appropriate, since the rather sticky concrete will develop friction even without vertical normal pressure.

Wooden surfaces were created for angles of 10°, 20°, 30° and 40° inclinations. For each angle of inclination, 6 parallel paths were printed consisting of 3 layer heights of 10 mm. The results of the first series of tests showed that as the angle of inclination did increase, the ability for a printed strip to maintain its form decreased. For angles of 10 and 20 degree inclinations, the printed concrete maintained its shape both for when printing up along the surface as well as downwards direction. For higher angles, the concrete was unable to maintain its shape, particularly when printing in a downwards direction. The concrete printed on the 30° inclination had a tendency to twist along itself until failure while concrete printed at an inclination of 40° rolled within itself in a ball-like fashion (Figs. 12–13).

Fig. 12. Initial print tests on slope inclinations.

6. Shell prototype: form finding

The results obtained in Section 6 were used as the constraints for form-finding of the final prototype. As it was intended to remain focused on the printer limitations, structural optimization was not taken into consideration during these cases. Form-finding was carried out using *Karamba3D*, a 2D FEM Analysis plugin for Grasshopper. An initial square geometry was deformed under its self-weight. A series of shells were analyzed and the chosen shape was that which had the maximum acceptable slope angle of 30° at any point along its surface.

A series of interlocking panels were imagined for the division of the shell geometry. These were defined by increasing the number of subdivisions in square panels and adding notches at these changes. All changes in direction were then filleted with the minimum turning radius of 100 mm found in Section 6.

The shell was panelized by projecting a 2D line drawing onto the curved surface as shown in Fig. 14. The individual panels were converted into print paths using the techniques described in Section 4. In order to increase the accuracy of the final prints, a CNC-Milled High-Density EPS mould was used as a representation of the flexible mould. A silicone sheet was laid on the entire surface of the EPS so as to have the same surface finish as the flexible mould.

6.1. First prototype

The first printed prototype consisted of a shell defined by 9 interlocking panels. This initial layout was chosen to maintain panels at a

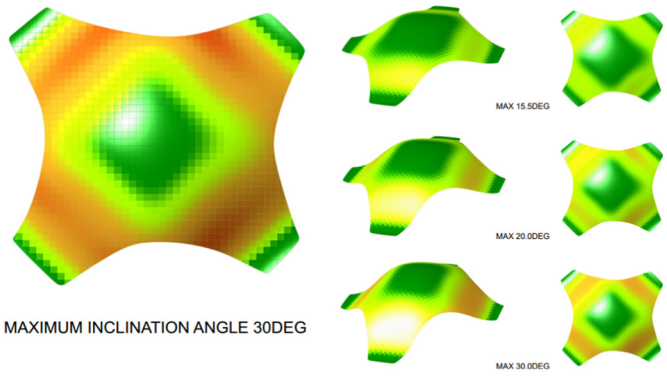

Fig. 13. Form-Finding processes for maximum curvature.

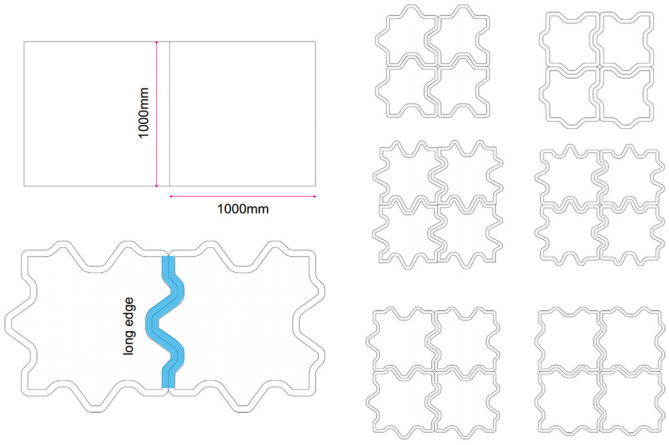

Fig. 14. Study of panel curvatures.

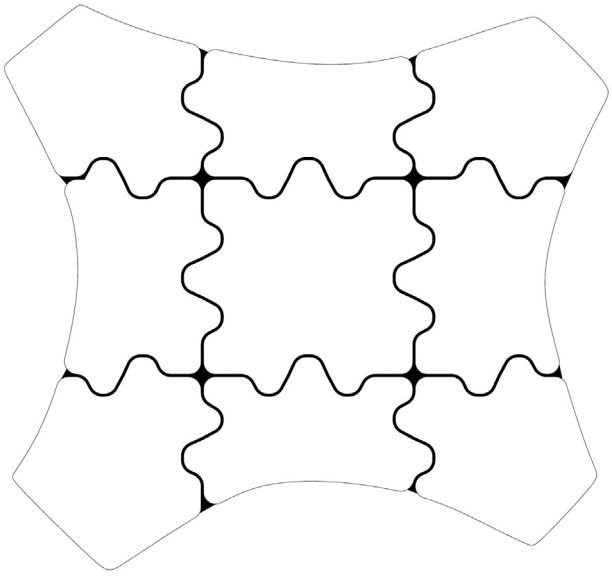

Fig. 15. Pavilion prototype panel tessellation.

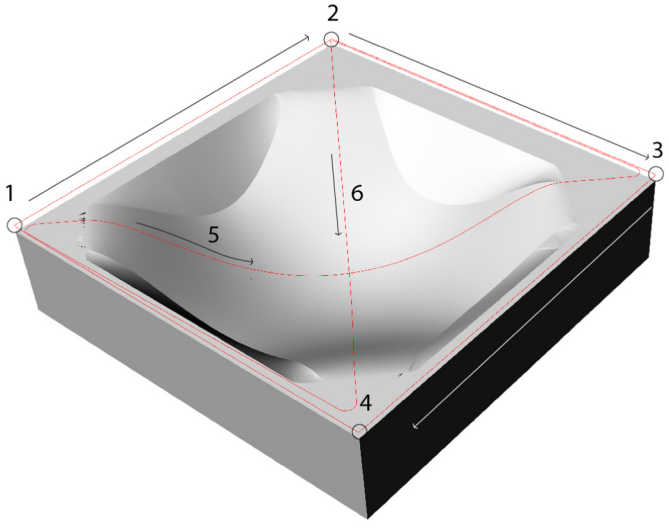

Fig. 16. Orientation strategy of temporary mould.

Fig. 17. Printing of the first prototype.

size less than 1000 mm × 1000 mm to allow for easy transportation (Figs. 15–16).

6.1.1. *Orienting the mould*

Printing of the prototype began with first referencing the position of the physical mould to the origin of the 3D Printer. The mould was positioned in an arbitrary point in physical space and the printer was then positioned at a specified origin point of the mould. Preliminary orientation is complete once the printer passes through points 2, 3 and 4 at which point it is established that the digital model is properly referenced to the physical model. An additional orientation path, travelling through paths 5 and 6, is included to double check that the printer follows the surface of the mould.

6.2. *Printed prototype*

The printed prototype had a layer height of 10 mm and width of 50 mm for a total of 3 layers. The Printing height was maintained between 15 mm and 25 mm. The same concrete used for printing was mixed with plasticizer and used for casting in between the printed outlines. The amount of plasticizer used was determined by judgement of the consistency of the concrete after it was mixed. A total printing time of roughly 15 min was needed for the first print and a further 20 min for filling the printed panels with concrete. Once completely printed and cast, the element was covered with a plastic sheet and left to cure in air for 24 h before demolding.

The results of the first large-scale print yielded a number of areas for improvement. Firstly, the print was carried without the use of the correction script described in Section 5. The effect of this is particularly evident in Fig. 17 above. Notable creasing occurred in areas where the printing height was too high. Moreover, the offset between panels was not sufficient and the printer nozzle impacted printed filament in certain areas during the printing process. The turning radius used also proved to be too low in certain areas, particularly when printing on the steeper angles. As seen in Fig. 18, many of the filleted edges were uneven and creased. This was due to the printer slowing down and rotating around sharp corners.

7. Final pavilion

A number of modifications to the shell geometry were carried out based on the findings of the first printed prototype. In order to ensure a continuously smooth print path, the minimum turning radius was increased to 150 mm. The implications of this meant that the panels would have to be increased in size in order to allow for correct filleting. Thus, the number of panels was reduced from 9 to 5: 4 perimeter panels and one central *keystone*. While this had implications on the transportability of the pieces, the maximum panel dimension was still at a reasonable 1200 mm. The advantage of reducing the number of panels also allowed for easier erection. Moreover, the correction script described in Section 7 was adopted for the printing of this shell. The offset between panels was also increased to 20 mm to ensure that the printer

Fig. 18. Printing of first prototype.

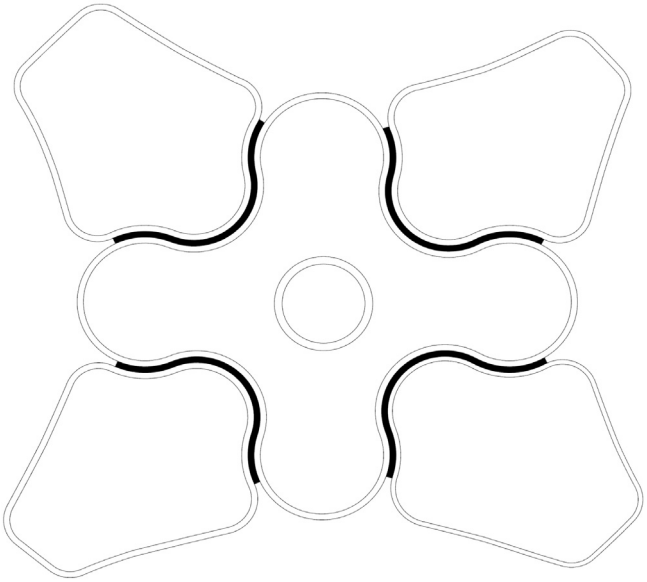

Fig. 19. Plan of final pavilion.

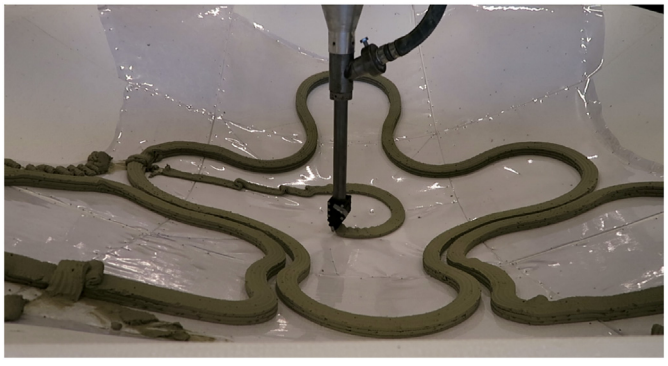

Fig. 20. Printing of final pavilion.

Fig. 21. Demolded final pavilion.

Fig. 22. Assembly of final shell.

Fig. 23. Seam between two panels indicating a tight fit.

would not collide during the printing as well as to allow for a greater degree of tolerances during construction. Because the structure had to be demountable, panels were fixed together by compression only, separated by a strip of 25 mm celrubber. The final pavilion also had a considerably faster printing time of 8 min. Casting of the panels was carried out in the same manner as described in Section 6.2. The structure was left to air-cure for 3 days before demolding to ensure adequate strength development. The print quality was far superior to the previous pavilion, largely due to a smoother printing path achieved by the correction script and increased minimum turning radius. As seen in Figs. 20 and 21, the larger turning radii allowed the printer to maintain a constant print speed and as a result a higher degree of accuracy was obtained in the final print (Fig. 19).

Fig. 24. Final shell structure realized.

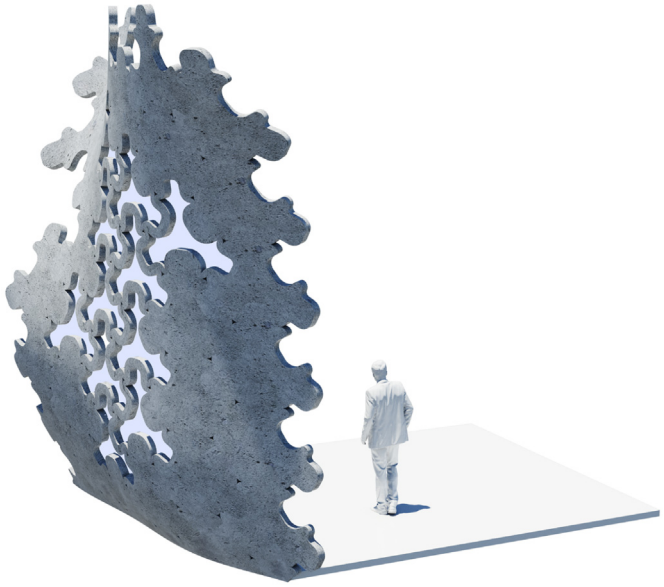

Fig. 25. Application of process as free-form cladding systems.

8. Assembly

25 mm half-density celrubber was inserted in between panels and compressed to 20 mm when loaded. This allowed for the panels to be self-supporting without the need for additional mechanical fixings and bolts, allowing for easy assembly and disassembly when required.

The structure was fixed to the wooden floor by means of 2 50 mm steel angles per panel. These were used to transfer the horizontal thrust forces without the need for tying.

The assembly sequence utilized is as follows:

a. Central Piece temporarily is propped up roughly in the center of the wooden platform.
b. First (*arbitrary*) panel is positioned to fit into position including the rubber strip. The steel angles for the panel are bolted into its position.
c. Adjacent panel to the first panel is positioned and fit to allow for more stability. The corresponding steel angles are also bolted into position.
d. The procedure is repeated until all 4 panels are positioned.
e. Panels are adjusted (rotated/elevated/depressed) in order to maintain a proper snug fit. This is an iterative process as the movement of one panel has a tendency to dislodge others (Fig. 22).

9. Discussion and recommendations

The final prototype had a relatively smooth surface finish due to casting on a silicon sheet. Although a number of seams are present where the milled blocks of foam joined together, it may be overcome by using a large-scale adaptable/milled mould for future projects. Moreover, the degree of accuracy reached was reasonable. As seen in Fig. 23 the seam between the panels is maintained at a tight fit. The total fabrication time (Printing and Casting) of the entire shell took less than an hour to complete, showing the potential for this method to be used as a method for fabrication complex elements with a good degree of accuracy (Fig. 24).

A number of recommendations for future studies can be identified from the outcome of this research. These are presented as follows:

- Incorporating 3D Scanning into the printing process. The original intent of the study was to include an additional step in the digital workflow to allow for the 3D Scanning of an element. However, due to time and resource constraints it was omitted from the final result. The use of scanning is beneficial to the project in a number of ways
  a. It is imagined that scanning will allow for a check between the accuracy of the digital model and the physical mould. In combination with projection mapping, areas on the physical mould which do not correspond with the digital model can be highlighted and adjusted
  b. By using real-time scanning of the adjusted mould described in point a would be beneficial to allow for a consistent nozzle offset distance and thus, a higher quality final print.
  c. Alternatively, an adjusted mould could be scanned and referenced back into Rhino. The surface formed from the point cloud could be used for creating the original print paths for more accurate printing. The drawback in such a method is that the entire physical model would have to be constantly updated to cope with the changes in printed panels
- Geometry informed through structural optimization. The forms studied for this paper were generated using the variables described in Section 8. A next step development would be to generate print paths based on structural analysis as already displayed by Tam et al. [1] and Stress Line Additive Manufacturing.
- Study using 6-Axis Robot. The main benefit of using a 6-Axis articulated arm is that nozzles can be oriented perpendicular to the surface, giving far more freedom in complexity of surfaces that can be used for printing on. The drawback in this setup, however, is that obtaining smooth movement required for printing is more troublesome. Moreover, wrist servo angles are generally restricted to −180 to 180°, meaning that nozzles may not always be able to be oriented perpendicular to the path direction.

10. Conclusion

This paper presented a novel method of Fused Depositioning Modelling-based 3D Concrete Printing, by printing and casting the object on an adaptable double curved surface, rather than a flat plane. This allows a new level of complexity to the geometries that can be manufactured with either technology (printing or casting on curved surfaces) separately. As a case study, a 5 m^2 self-supporting, double curved shell that consisted of multiple panels was designed, produced and assembled.

To allow this, an automated single file workflow from design to production was developed, using Grasshopper. This required several innovations, including an alternative method to generate the appropriate g-code to account for the continuous linear nature of the filament on a double curved print bed. Another issue that needed an adapted strategy was the non-constant surface-to-nozzle distance, which is caused by the fact that the robot is limited to 4 DOFs. As this depended on the varying inclination of the mould, a local correction script was

applied to the generated g-code path. Further investigations targeted the physical aspects of printing concrete onto curved inclined surfaces. The maximum inclination angle without sliding or otherwise distorting the filament was established at 30°. The minimum turning radius on a flat plane was 100 mm, but this increased to 150 mm on inclined surfaces. These constraints were included in the shell design. To minimize these difficulties associated with the printing on a double curved surface with a 4 DOF printer, an orientation optimization was performed so that the inclination of each panel during printing would be minimal.

When printing on a flat x, y-plane, only the z-position of the print table relative to the print nozzle needs to be calibrated. In this study, however, also the x and y-positions, as well as the rz orientation, needed calibration to allow a correct print. For this, too, a method was developed. Hence it may be concluded that the introduction of a non-planar print bed to 3D Concrete Printing requires a significantly more sophisticated workflow to account for the effects of geometry on instrument compatibility and physical behavior of the print material.

The project has shown that, once the appropriate workflow has been established, it is feasible to realize relatively complex freeform panels accurately, fast, and with little material waste. Currently, it is foreseen that the particular arrangement is beneficial for creating free-form, 2.5D structures panel-like structures, such as bespoke concrete cladding systems (Fig. 25) or segmented shell elements as already demonstrated in the paper. The combination of printing and casting results in a typology quite different from what we generally see produced by 3D concrete printers today.

Author contributions

The manuscript was written through contributions of all authors. All authors have given approval to the final version of the manuscript.

Funding sources

The research carried out in this paper was fully funded by the call 3TU.Bouw Lighthouse projecten 2016 https://www.4tu.nl/en/.

Acknowledgments

The Authors of the paper would first and foremost like to thank the 4TU Federation for fully-funding the project for its duration. Gratitude is further extended towards all lab staff at the Printing Lab at TU Eindhoven. We would like to also express our gratitude to all MSC students at the faculty at TU Eindhoven that helped with printing throughout the past year.

Appendix A

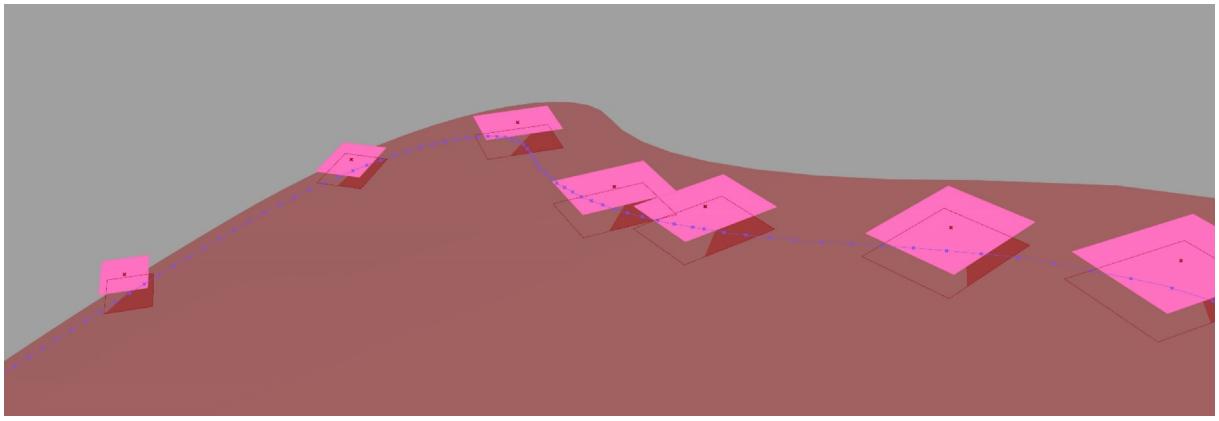

Reference: Section 7. Grasshopper correction script showing sampled points for height adjustment

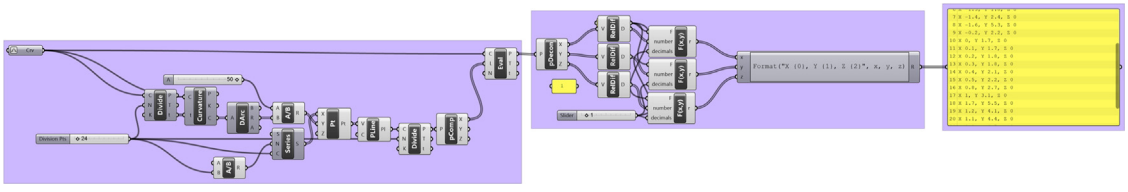

Reference: Section 7. Principle for generating co-ordinates for communicating with printer

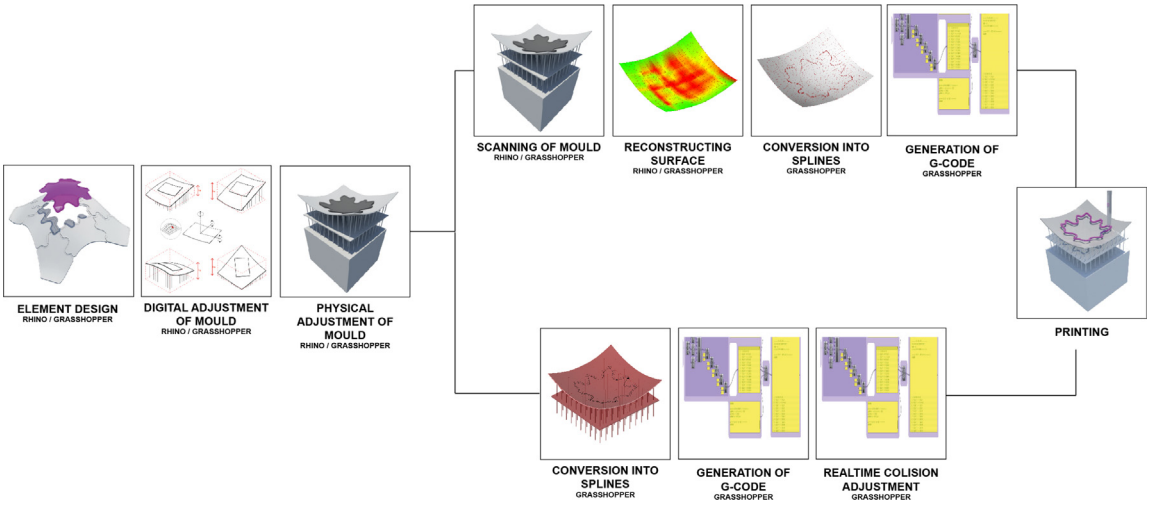

Reference: Section 7 - digital workflow

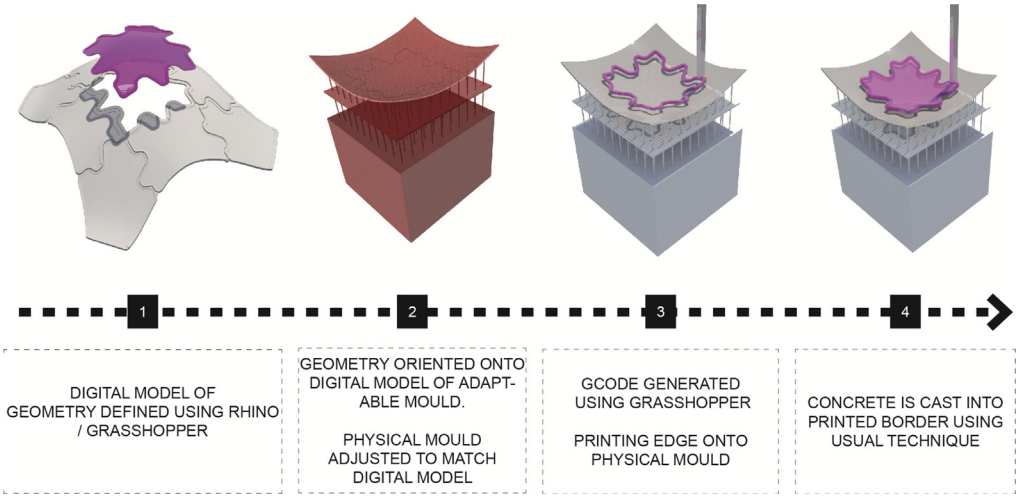

Reference: Section 7 – production process

References

[1] K. Tam, J. Coleman, N. Fine, C. Mueller, Stress line additive manufacturing (SLAM) for 2.5-D shells. Digitalstructures.Mit.Edu, (August), Retrieved, 2015. http://digitalstructures.mit.edu/files/2015-07/iass2015-final-slampaper.pdf.

[2] A. Seyedahmadian, O.O. Torghabehi, W. Mcgee, Developing a computational approach towards a performance based design and robotic fabrication of fibrous skin structures, Proceedings of the International Association for Shell and Spatial Structures (IASS) Symposium. 17–20 August 2015; Amsterdam, The Netherlands, 2015 http://www.ingentaconnect.com/content/iass/piass/2015/00002015/00000002/art00013.

[3] M. Doerstelmann, J. Knippers, V. Koslowski, A. Menges, M. Prado, G. Schieber, L. Vasey, ICD/ITKE research pavilion 2014–15: fibre placement on a pneumatic body based on a water spider web, Archit. Des. 85 (5) (2015) 60–65 Retrieved https://doi.org/10.1002/ad.1955.

[4] Dini, E. (2016). Available online. D-Shape. Retrieved from http://d-shape.com/. (Accessed June 2017).

[5] H.R. Schipper, Double-curved Precast Concrete Elements - Research Into Technical Viability of the Flexible Mould Method, (2015), https://doi.org/10.4233/uuid:cc231be1-662c-4b1f-a1ca-8be22c0c4177.

[6] C. Borg Costanzi, M. Bilow, U. Knaack, 3D Printing concrete on temporary surfaces (Master Thesis). Retrieved from, 2016. https://repository.tudelft.nl.

[7] F. Bos, R.J.M. Wolfs, Z.Y. Ahmed, T. Salet, Additive manufacturing of concrete in construction: potentials and challenges of 3D concrete printing, Virtual and Physical Prototyping, 11:3 2016, pp. 209–225, https://doi.org/10.1080/17452759.2016.1209867.

[8] Adapa, Available online http://adapa.dk, (2018), Accessed date: 21 May 2018.

[9] F. De Larrard, Why rheology matters, Concr. Int. 21 (8) (1999) 79–81 Retrieved https://www.concrete.org/publications/internationalconcreteabstractsportal/m/details/id/270.

[10] J.E. Wallevik, Relationship between the Bingham parameters and slump, Cem. Concr. Res. 36 (7) (2006) 1214–1221 Retrieved https://doi.org/10.1016/j.cemconres.2006.03.001.

[11] F.V. Mueller, K. Khayat, O. Wallevik, Linking Yield Stress of a Co-Axial Cylinders Viscometer and Parameters of Consistency Testing Using the Abrams Cone. (Conference Paper) International Symposium on Environmentally Friendly Concrete - ECO-Crete; 13–15 August 2014; Reykjavik, Iceland, (2014) https://www.researchgate.net/publication/318573236.

[12] S. Lim, R.A. Buswell, P.J. Valentine, D. Piker, S.A. Austin, X. De Kestelier, Modelling curved-layered printing paths for fabricating large-scale construction components, Loughborough University, 2016 Retrieved from https://dspace.lboro.ac.uk/dspace-jspui/handle/2134/21980.

[13] K.J. Vollers, Making 3D Façades: the pinbed, (2013) retrieved from http://materia.nl/article/making-3d-facades-the-pinbed/ last visited June 2018.